



PCCP

## ZSM-5 Decrystallization and Dealumination in Hot Liquid Water

Journal:	<i>Physical Chemistry Chemical Physics</i>
Manuscript ID	CP-ART-03-2019-001490.R1
Article Type:	Paper
Date Submitted by the Author:	16-Jul-2019
Complete List of Authors:	<p>Maag, Alex; Worcester Polytechnic Institute, Chemical Engineering  Tompsett, Geoffrey; Worcester Polytechnic Institute, Chemical Engineering  Tam, Jason; University of Toronto, Materials Science and Engineering  Ang, Cheen Aik; University of Toronto, Chemical Engineering  Azimi, Gisele; University of Toronto, Chemical Engineering  Carl, Alexander; Worcester Polytechnic Institute, Chemistry and Biochemistry  Huang, Xinlei; Syracuse University, Biomedical and Chemical Engineering  Smith, Luis; Clark University  Grimm, Ronald; Worcester Polytechnic Institute, Chemistry and Biochemistry  Bond, Jesse; Syracuse University, Biomedical and Chemical Engineering  Timko, Michael; Worcester Polytechnic Institute, Chemical Engineering</p>

SCHOLARONE™  
Manuscripts

# ZSM-5 Decrystallization and Dealumination in Hot Liquid Water

*Alex R. Maag<sup>†</sup>, Geoffrey A. Tompsett<sup>†</sup>, Jason Tam<sup>‡</sup>, Cheen Aik Ang<sup>‡</sup>, Gisele Azim<sup>#</sup>,  
Alexander D. Carl<sup>†</sup>, Xinlei Huang,<sup>§</sup> Luis J. Smith<sup>‡</sup>, Ronald L. Grimm<sup>†</sup>, Jesse Q. Bond,<sup>§</sup>  
Michael T. Timko<sup>\*†</sup>*

<sup>†</sup>Department of Chemical Engineering at Worcester Polytechnic Institute, 100 Institute  
Road, Worcester, Massachusetts 01609, USA

<sup>‡</sup>Department of Chemical Engineering and Applied Chemistry and Material Sciences  
and Engineering, University of Toronto, Toronto, Ontario M5S 3E5, Canada

<sup>§</sup>Department of Biomedical and Chemical Engineering, Syracuse University, 329 Link  
Hall, Syracuse, NY 13244

\*Department of Chemistry, Clark University, 950 Main Street, Worcester MA 01610,

USA

**Abstract.**

Zeolites have recently attracted attention for upgrading renewable resources in the presence of liquid water phases; however, the stability of zeolites in the presence of liquid-phase water is not completely understood. Accordingly, the stability of the ZSM-5 framework and its acid sites was studied in the presence of water at temperatures ranging from 250 to 450 °C and at pressures sufficient to maintain a liquid or liquid-like state (25 MPa). Treated samples were analyzed for framework degradation and Al content and coordination using a variety of complementary techniques, including X-ray diffraction, electron microscopy, N<sub>2</sub> sorption, <sup>27</sup>Al and <sup>29</sup>Si NMR spectroscopy, and several different types of infrared spectroscopy. These analyses indicate that the ZSM-5 framework retains >80% crystallinity at all conditions, and that 300-400 °C are the most aggressive. Decrystallization appears to initiate primarily at crystal surfaces and share many characteristics in common with alkali promoted desilication. Liquid water treatment

promotes ZSM-5 dealumination, following a mechanism analogous to that observed under steaming conditions: initiation by Al-O hydrolysis, Al migration to the surface, and finally deposition as extra framework Al or possibly complete dissolution under some conditions. As with the framework, dealumination is most aggressive at 300-400 °C. Several models were evaluated to capture the non-Arrhenius effect of temperature on decrystallization and dealumination, the most successful of which included temperature dependent values of the water auto-ionization constant. These results can help interpretation of previous studies on ZSM-5 catalysis in hot liquid water and suggest future approaches to extend catalyst lifetime.

Keywords: ZSM-5, dealumination, desilication, hot liquid water, supercritical fluid, dielectric constant, water self-dissociation constant, Arrhenius analysis

## 1. Introduction

Interest in the use of zeolites as solid acid catalysts in liquid water has intensified in recent years, driven largely by the search for renewable alternatives to petroleum feedstocks for fuels and chemicals production.<sup>1</sup> Performing chemistry transformations in

the presence of liquid water can reduce the energy required for processing wet feeds that require drying if processed using non-aqueous techniques.<sup>1, 2</sup> Similarly, several studies have demonstrated that zeolites, in particular ZSM-5, promote formation of gases, short-chain alkanes, and aromatics from upgrading of fatty acids, algae bio-oil, and vegetable oil in liquid water at temperatures near or greater than its critical point (374 °C).<sup>3-6</sup> For example, Deepa et al.<sup>7</sup> found that zeolites improve lignin de-polymerization to form aromatics at 250 °C in the presence of hot liquid water, but reported limited catalyst reusability. Similarly, Mo et al.<sup>8</sup> found ZSM-5 to be active for conversion of palmitic acid into an aromatic rich bio-oil, again under supercritical water conditions and again with only partial retention of activity on reuse.

Despite technological interest, many fundamental questions about the role of water on zeolite stability remain incompletely understood in the liquid phase.<sup>9-18</sup> Previous work suggests that MFI is the most stable of the common zeolite frameworks in the presence of hot liquid phase water, with studies showing that it retains crystallinity for 6 h in liquid water at temperatures as great as 200 °C.<sup>10, 11</sup> In comparison, other frameworks undergo substantial degradation at similar conditions.<sup>11, 13, 17, 18</sup>

A growing number of studies examine the activity of MFI and other zeolites at temperatures much greater than its known limits of stability.<sup>5, 7, 8, 19</sup> In fact, reports of reduced activity<sup>19</sup> and reduced reusability<sup>8</sup> in the presence of hot liquid water might plausibly be due to water-promoted zeolite degradation; however, making this assertion cannot be conclusive due to the lack of stability data over the temperature range where catalysis has been studied most actively.

Adding to the uncertainty introduced by zeolite degradation during reaction, several recent studies suggest that ZSM-5 degradation products, including soluble aluminum and nanosized aluminosilicate fragments, act as the catalyst under aqueous-phase conditions, rather than the zeolite itself.<sup>20, 21</sup> Zaker et al.<sup>19</sup> evaluated the activity of putative ZSM-5 breakdown products such as silicalite, alumina, and many others before concluding that ZSM-5 retains heterogeneous acidity in the presence of supercritical water and that none of the homogeneous or heterogeneous degradation products could explain the observed activity. Most studies do not mention performing the control studies required to rule out the potential activity of ZSM-5 degradation products, meaning that interpretation of literature studies remains uncertain. Moreover, future studies would

benefit from a more comprehensive understanding of the limits of ZSM-5 stability in hot liquid water, better quantification of its stability relative to other zeolites, and greater insight into the mechanism of ZSM-5 degradation and the role of water-zeolite interactions.

To address these gaps in our understanding, ZSM-5 was treated for 3 hours in hot liquid water at temperatures ranging from 250 to 450 °C. These temperature and time conditions were selected based on previous work by Zaker et al.<sup>19</sup> that reported that ZSM-5 crystallinity decreased by 20% when exposed to a mixture of dodecane and supercritical water at 400 °C for 2 hours. Accordingly, 3 hours represents a likely intermediate time point in the ZSM-5 degradation pathway. Post-run characterization tests evaluated changes in framework crystallinity, textural properties, and aluminum coordination, content, and distribution. These data were first evaluated to quantify the stability of ZSM-5 and draw comparisons with literature on steam, acid, and alkali treatments to understand the degradation mechanism of ZSM-5 in hot liquid water. Next, degradation rates were analyzed using several different types of Arrhenius models to examine the effects of water-zeolite interactions. These results and analysis advance the current understanding

of zeolite degradation in liquid water and suggest new avenues for future work to stabilize zeolites in this important solvent.

## 2. Experimental Section

**2.1 Materials.** Binderless ZSM-5 zeolite powder (2  $\mu\text{m}$  crystals) with Si/Al=38 was obtained from ACS Materials. Prior to use, catalysts were heated to 100  $^{\circ}\text{C}$  for at least one hour followed by calcination at 550  $^{\circ}\text{C}$  for at least 16 hours under ambient air conditions. Water was deionized to 17.9  $\text{M}\Omega\text{ cm}$  prior to use.

**2.2 Catalyst Stability Experiments.** Catalyst stability tests were performed in a pressurized flow-through reactor. A detailed description of the catalytic packed bed setup is provided in the Supporting Methods. At the start of each experiment, the oven temperature was increased to the desired set point while maintaining a constant nitrogen flow through the reactor. A nitrogen flow was used during heat-up (and cool-down) to provide careful control of the temperature history of the zeolite when exposed to liquid water.<sup>22</sup> Upon reaching the desired operating temperature, de-ionized water was pumped into the system at a flow rate of 4  $\text{ml min}^{-1}$  (Eldex, Optos pump). The water was maintained in the liquid state using a back pressure regulator (Equilibar H6P) set to 25

MPa, which is greater than the critical pressure of water. The water was fed sequentially through the preheat tubing, catalyst tube, chilled tubing section, and 2 filters (15 and 2  $\mu\text{m}$ ) before exiting the system. After 3 hours, the water flow was discontinued and nitrogen was used to expel water from the reactor zone before cooling the system. The reactor was depressurized once the temperature reached 60 °C.

**2.3 Material Characterization.** ZSM-5 was characterized before and after hydrothermal treatment using a range of established techniques: scanning electron microscopy (SEM) and energy dispersive x-ray spectroscopy (EDS), X-ray diffraction (XRD),  $\text{N}_2$  adsorption, transmission electron microscopy (STEM), X-ray photoelectron spectroscopy (XPS), diffuse reflectance infrared Fourier transform spectroscopy (DRIFTS),  $^{29}\text{Si}$  and  $^{27}\text{Al}$  solid-state NMR, temperature-programmed surface reactions of isopropylamine, and Fourier transform infrared (FTIR) spectroscopy of ZSM-5 with adsorbed pyridine. Detailed descriptions of all characterization techniques are included in the methods sections of the Supporting Information.

### 3. Results

Previous work suggests that MFI is the most stable common zeolite framework in the presence of hot liquid water.<sup>11, 13, 17, 18</sup> Nonetheless, many studies have outstripped our knowledge of MFI stability to examine ZSM-5 activity at temperatures where no stability data exist. This study consists of two components. The first component is an experimental study to examine the effects of hot liquid water treatment on the properties of ZSM-5 over the entire range of temperatures where its activity has been evaluated. The second component, described in the Discussion, is analysis of these results to understand the effects of water-zeolite interactions on zeolite degradation.

For the experimental component of this study, ZSM-5 with an initial Si/Al ratio equal to 38:1 was selected for study, similar to the composition of ZSM-5 used previously for catalysis.<sup>4, 5, 8</sup> Moreover, computational methods<sup>23</sup> and experimental studies have found ZSM-5 stability to be weakly dependent on Al content and optimized in the range from 25 to 100. Tests were performed over the temperature range from 250 to 450 °C and 25 MPa to cover the entire temperature range where ZSM-5 catalysis has been studied in liquid water. The pressure was selected to maintain water as a liquid, subcritical, or dense supercritical phase conditions, with the density of water varying smoothly but non-linearly

from  $0.82 \text{ g cm}^{-3}$  at  $250 \text{ }^\circ\text{C}$  to  $0.11 \text{ g cm}^{-3}$  at  $450 \text{ }^\circ\text{C}$ .<sup>24</sup> Treated samples were subsequently analyzed for changes in crystallinity, textural properties, and acid site density to assess the degradation of the zeolite framework (Section 3.1) and aluminum composition and coordination (Section 3.2) during treatment in hot liquid water.

### 3.1 Framework Stability

XRD has been used to evaluate retained crystallinity of water-treated zeolites in several previous studies<sup>10, 11, 13</sup> and has become a benchmark measurement of stability. Figure 1a shows representative XRD data for calcined ZSM-5 and ZSM-5 treated in hot liquid water for 3 hours at temperatures ranging from 250 to  $450 \text{ }^\circ\text{C}$ . The sharp diffraction peaks associated with the MFI framework are apparent in all spectra, suggesting that ZSM-5 retains at least partial crystallinity even after treatment at  $450 \text{ }^\circ\text{C}$ . Likewise, no new peaks appear after treatment, suggesting that water treatment does not promote formation of new crystalline phases.

Figure 1b provides degree of crystallinity data determined by integration of ZSM-5 crystalline peaks ( $22.5\text{--}25 \text{ }2\theta$  degrees) using the ASTM Standard D5758,<sup>25</sup> which was found to be reproducible to within  $\pm 3\%$  and has a reported 95% reproducibility interval of  $\pm 5.04\%$ .<sup>25</sup> At

temperatures less than 325 °C, crystallinity loss is less than the estimated limits of experimental uncertainty based on repeated experiments at every condition. The new data are consistent with prior studies of ZSM-5 degradation in liquid water which examined behavior at temperatures up to 200 °C, as shown in Figure 1b.<sup>10, 11</sup> At temperatures greater than 325 °C, ZSM-5 crystallinity decreases by 10 to 20%, reaching a minimum retained crystallinity of about 80% at a temperature of 420 °C. At temperatures greater than 420 °C, ZSM-5 retains >90% of its original crystallinity. Interestingly, the crystallinity minimum coincides roughly, but not exactly, with the critical temperature of water (374 °C).

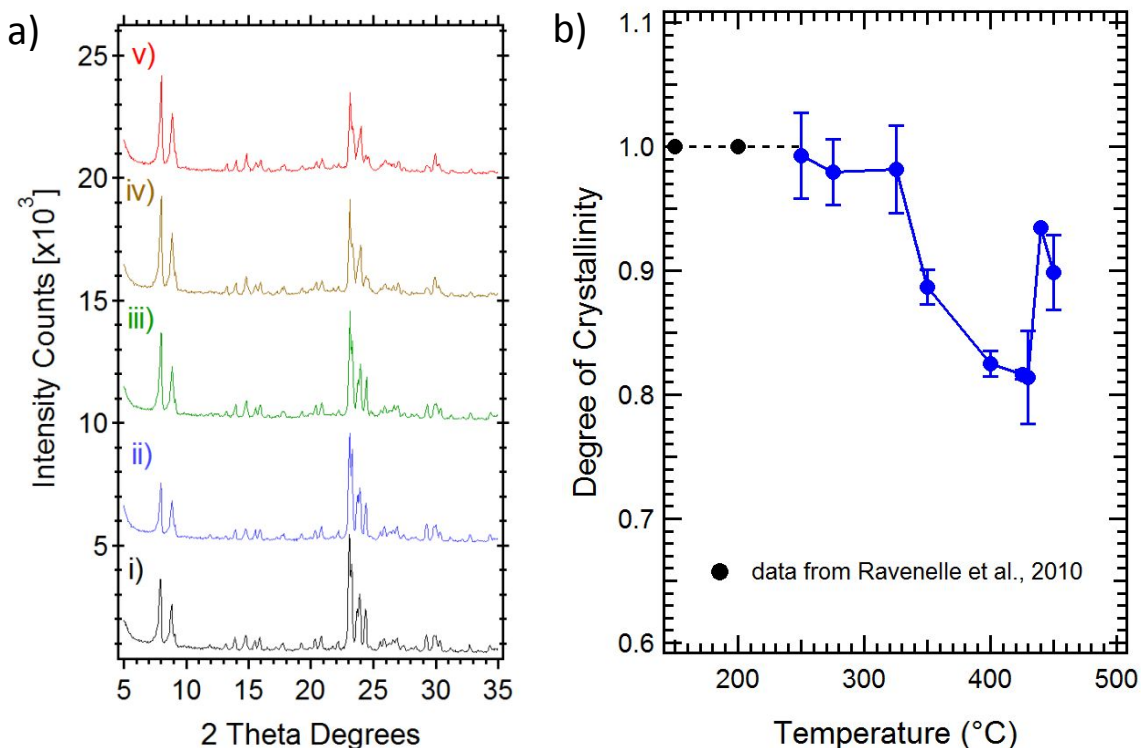


**Figure 1.** (a) XRD pattern of ZSM-5 samples of (i) calcined and (ii-v) hydrothermally treated samples for three hours at 250 °C, 325 °C 400 °C and 450 °C respectively. (b) Corresponding degree of crystallinity for ZSM-5 calculated between 22.5-25.0 2 $\theta$  degrees at different treatment temperatures relative to a reference calcined ZSM-5, ● are from Ravenelle et al.<sup>11</sup> for ZSM-5 at a Si/Al ratio between 15-40.

The observed temperature dependence of framework degradation is unusual and, assuming that the data reflect degradation rates, stand in apparent contradiction to the well-established Arrhenius relationships between reaction rate and temperature.<sup>26</sup> The

observation was consistent over multiple, independent experiments, mitigating doubt of its reproducibility. No evidence for formation of new crystalline phases was observed, removing formation of a new, more stable phase at  $>400$  °C as a possible explanation. The crystallinity loss at  $450$  °C was slightly greater than at  $440$  °C, suggesting resumption of the expected Arrhenius behavior after the aforementioned disruption occurring over the temperature range from  $375$  to  $425$  °C. A natural response to the discovery of an unexpected relationship between crystallinity retention and temperature is to question the experimental method. The typical response to this uncertainty is utilization of complementary techniques to examine the phenomenon from multiple perspectives, and the next steps of this work involved characterizing the water-treated zeolite using electron imaging and gas sorption.

Electron imaging can provide qualitative insight into zeolite degradation mechanisms.<sup>13</sup>

Figure 2 shows representative SEM micrographs obtained from imaging calcined zeolite (a) and zeolites treated in liquid water at  $250$  (b),  $325$  (c), and  $450$  °C (d). The calcined ZSM-5 consists of  $\sim 2$   $\mu\text{m}$  crystallites with smooth surfaces and sharp edges, typical features reported for commercial zeolites.<sup>11, 13, 27</sup> The crystal sizes of the sample treated

at 250 °C are similar to the original material, albeit with rounded edges and bearing surface cavities with diameters in the range of 50-100 nm, as highlighted in Figure 2b.

The surface cavities observed in samples treated at 250 °C are qualitatively similar to features arising under strong alkali conditions at treatment temperatures less than 100 °C, as observed by Groen et al.<sup>28</sup> Qualitative similarities in surface features between hot liquid water (250 °C) and alkali solutions (<100 °C) may suggest some similarities in mechanism, which is a topic of consideration later in this document.

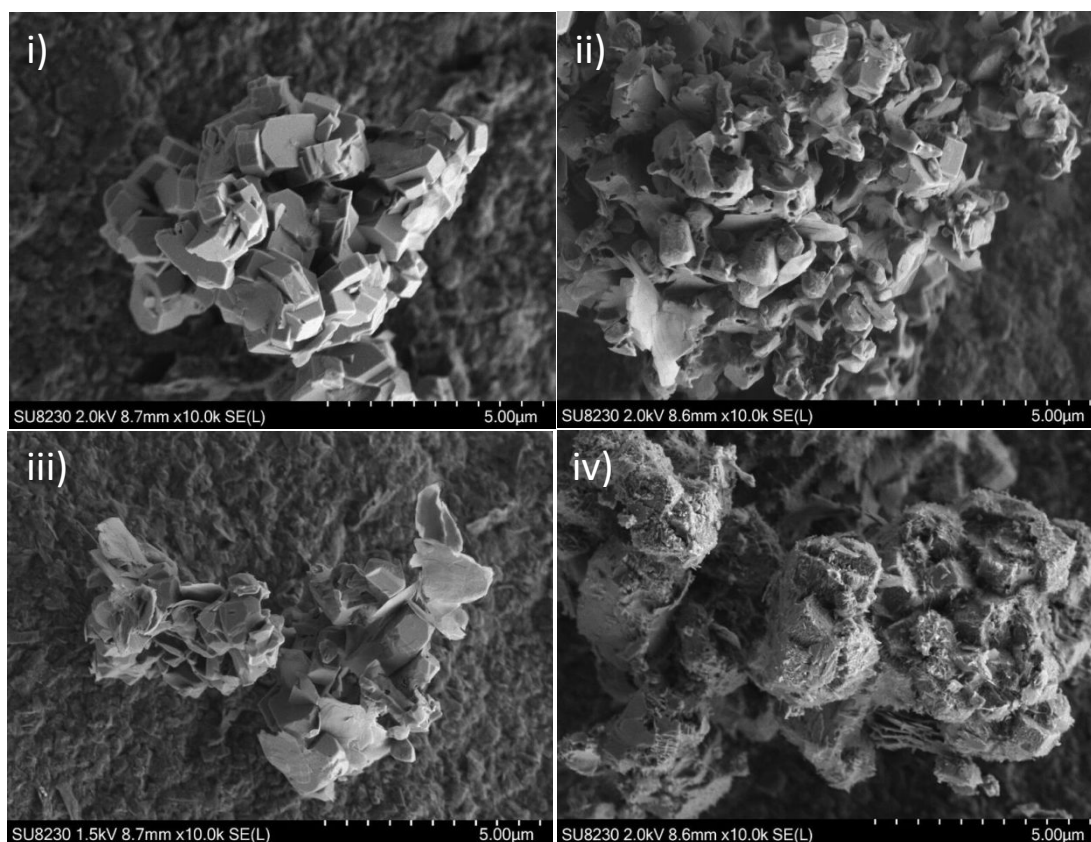


**Figure 2.** SEM images of ZSM-5 samples i) untreated, ii) 250 °C treated, iii) 325 °C and iv) 450 °C treated samples in hot liquid water. “a” and “b” dimensions are labeled in white to denote the change in crystal thickness

Unlike samples treated at 250 °C, which exhibit modest textural changes, ZSM-5 treated at 325 °C (Figure 2c) undergoes noticeable degradation, with zeolite crystals decreasing from approximately 0.5  $\mu\text{m}$  to approximately 100 nm in thickness. The observation of decreased particle thickness at 325 °C is consistent with the onset temperature of crystallinity loss shown previously in Figure 1b. The surfaces of ZSM-5 particles treated at 325 °C retain smooth edges and, unlike samples treated at 250 °C, do not exhibit surface cavities. Similar to the images obtained from particles treated a 325 °C in hot liquid water, Fodor et al.<sup>29</sup> reported preferential degradation of (010) facets after ZSM-5 treatment under alkali conditions, with subsequent formation of flat crystals. The surfaces of ZSM-5 particles treated at 450 °C are visibly rough with the appearance of nanoscale needle-like features. These qualitative features are consistent with aggressive

degradation, similar to images reported in previous studies of zeolite Y and  $\beta$  degradation in hot liquid water at much milder temperatures.<sup>11, 12, 16</sup>

SEM provides information on exterior surfaces whereas XRD is a bulk technique that is most sensitive to the particle interior. STEM has been used in previous studies to visualize the effects of liquid water treatment on the internal ZSM-5 framework, specifically the integrity of crystal lattices during the hot liquid water treatment.<sup>22, 28, 30, 31</sup> Figure 3 provides representative bright-field images obtained from STEM analysis of calcined ZSM-5 (3a) and samples treated in hot liquid water at 325 (3b), 400 (3c), and 450 °C (3d). The STEM image of calcined ZSM-5 reveals straight channels that lack any obstructions or blurriness, as expected for pristine MFI. After treatment at all temperatures, the internal lattice fringes of ZSM-5 retain their original straightness and remain intact and unbroken. A lack of blurriness or bumps in the internal lattice fringes of all treated samples strongly indicates that neither does the framework collapse during liquid water treatment nor does the water treatment induce formation of internal mesopores, unlike previous reports of water-treated H- $\beta$ .<sup>18</sup> Interestingly, internal features are retained even after treatment at

450 °C, consistent with retention of >80% of crystallinity at these conditions and lending credibility to the XRD results shown in Figure 1.

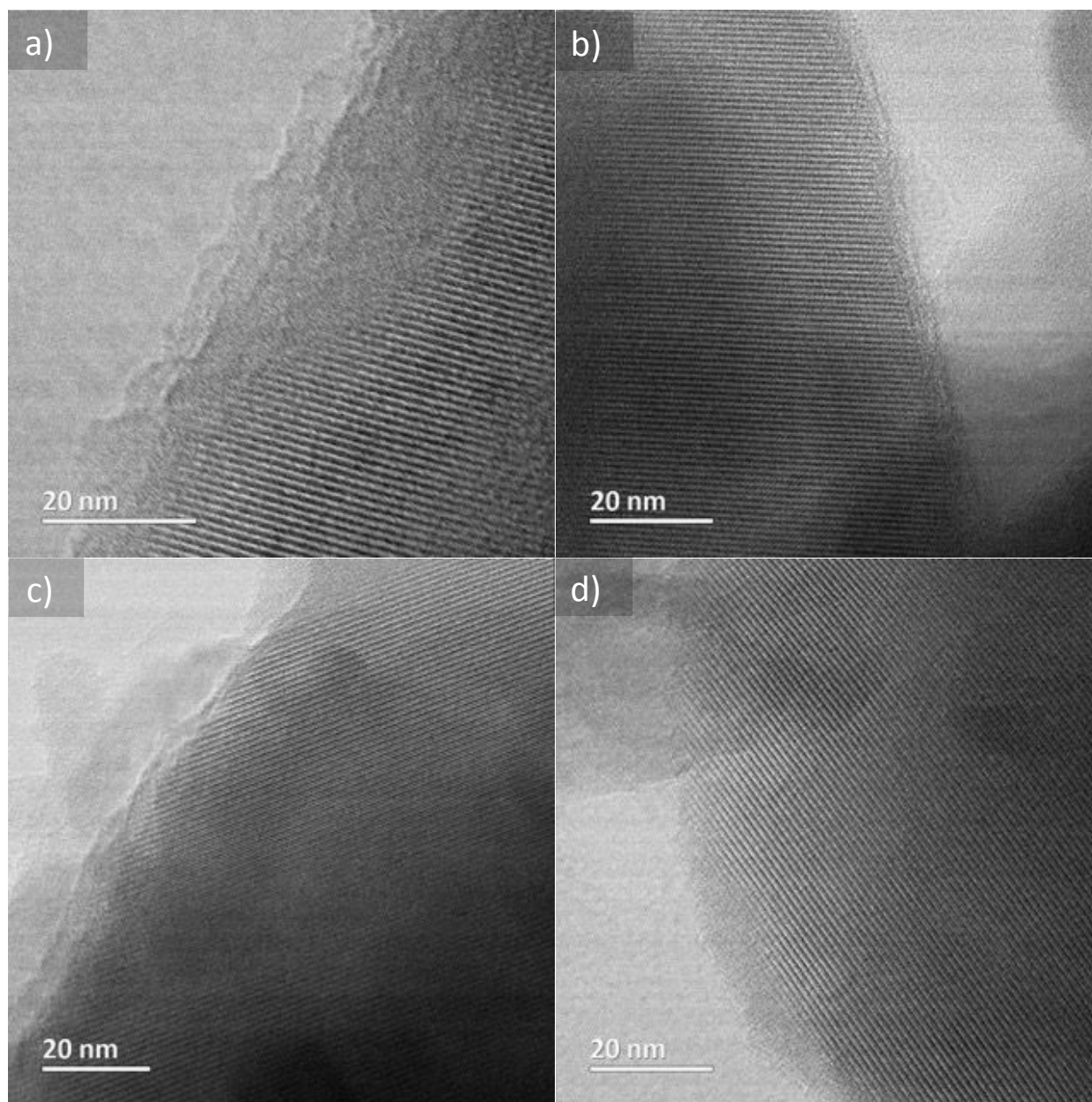


**Figure 3.** STEM images of ZSM-5 samples a) untreated, b) 325 °C treated, c) 400 °C treated and d) 450 °C treated samples in hot liquid water.

STEM analysis is consistent with XRD result, but is naturally limited by the number of images that can be obtained and analyzed. Accordingly, N<sub>2</sub> sorption was used as to investigate the effects of liquid water treatment on the bulk textural properties of ZSM-5, specifically surface area and micro/meso-porosity. Figure SI-1 (contained in the Supporting Information) shows representative N<sub>2</sub> isotherms obtained from analysis of ZSM-5 and samples treated in hot liquid water at various temperatures. In all cases, the N<sub>2</sub> sorption data appeared as IUPAC-type-II isotherms, consistent with the microporous characteristics of samples. Minor qualitative differences were present in the isotherms, but they do not influence the overall analysis. The Supporting Information provides more discussion.

Table 1 provides textural properties estimated from the N<sub>2</sub> sorption isotherms using the  $t$ -plot method.<sup>32</sup> The data in Table 1 indicate that micropore surface area,  $S_{t\text{-plot, micro}}$ , is not changed by treatment at 250 °C but decreases by approximately 40% after treatment at 275 °C. After treatment at temperatures greater than 275 °C, the micropore area increases monotonically with increasing treatment temperature, reaching a value of 286 m<sup>2</sup> g<sup>-1</sup> after treatment at 450 °C. The micropore area after treatment follows similar trends

as observed for crystallinity (Figure 1b), as increasing the treatment temperature did not lead to monotonic increases in zeolite degradation and instead exhibits a more complex relationship between zeolite degradation and temperature. Figure SI-2 in the Supporting Information contains plots of the total, micropore, and external surface area values as functions of retained crystallinity, showing the complex relationships that exist between these different zeolite characteristics. Most importantly, the data in Table 1 indicate retention of >60% of the original micropore area after treatment in liquid water and that the most aggressive conditions are temperatures between 300-400 °C. Both of these observations are broadly consistent with the XRD data shown in Figure 1b, which show retention of crystallinity and that the most aggressive conditions are found at 300-400 °C.

**Table 1.** Texture properties of ZSM-5 after hydrothermal treatment in liquid water at different temperatures.

Sample Treatment	Relative <sup>a</sup> Crystallinity	$S_{t\text{-plot, micro}}^b$ (m <sup>2</sup> /g)	$S_{t\text{-plot, ext}}^b$ (m <sup>2</sup> /g)	$S_{\text{micro}}/S_{\text{ext}}$ <sup>b</sup> ratio	$V_{\text{micro}}^b$ (cm <sup>3</sup> /g)	$V_{\text{meso}}^c$ (cm <sup>3</sup> /g)
Calcined	1.00	326	35.6	9.2	0.168	0.049
250 °C	0.99	350	138.3	2.5	0.183	0.19
275 °C	0.98	193	72.8	2.6	0.098	0.120
325 °C	0.98	221	62.6	3.5	0.113	0.096
350 °C	0.89	257	67.1	3.8	0.130	0.103
430 °C	0.81	285	58.8	4.8	0.141	0.088
450 °C	0.90	287	49.4	5.8	0.139	0.074

<sup>a</sup> Relative crystallinity from ratio of treated with calcined material; <sup>b</sup> micropore surface area and volume are calculated using the  $t$ -plot method; <sup>c</sup> mesopore volume is calculated from the difference between the micropore volume and the total volume at  $P/P_0 = 0.95$ .

In contrast with the internal surface area, the external surface area increases with increasing treatment temperature for temperatures less than 275 °C and then decreases gradually from 73 to 49 m<sup>2</sup> g<sup>-1</sup> over the range from 275 to 450 °C. The increase in external surface area observed for the sample treated at 250 °C may be consistent with the decreased particle thickness and formation of surface cavities observed using SEM

(Figure 2b). The decreasing external surface area observed with increasing temperature from 250 to 450 °C may be the result of inter-particle twinning.

### 3.2 Aluminum Stability

The next step was to study the fate of aluminum, and specifically the resulting effect on Brønsted acid sites (BAS) and Lewis acid sites (LAS). Interestingly, previous studies on zeolite degradation in liquid water have focused on decrystallization,<sup>10, 13, 17</sup> and the literature data on zeolite dealumination in hot liquid water are sparse. The focus of previous studies on decrystallization is natural since frameworks such as FAU and BEA decrystallize at rates too rapid to make study of dealumination meaningful. Fortunately, the literature on dealumination under steaming conditions is much more comprehensive and provides a guide for the current study.<sup>33-35</sup> Typically, studies on dealumination involve use of multiple different techniques to study quantitative and qualitative aspects of aluminum content, aluminum coordination, and aluminum location. Accordingly, <sup>27</sup>Al-NMR (and <sup>29</sup>Si-NMR), XPS, EDS, IR, and titration methods were used to develop a composite picture of dealumination.

$^{27}\text{Al}$  NMR was used to quantify bulk Al content and investigate the coordination of the aluminum atoms. Figure 4 shows  $^{27}\text{Al}$  NMR spectra obtained from analysis of calcined ZSM-5 and samples treated in hot liquid water. Figure SI-3 contains  $^{29}\text{Si}$  NMR data, which are consistent with the Al data shown in Figure 4. The  $^{27}\text{Al}$  NMR spectrum of the parent ZSM-5 contains a major peak at 60 ppm, attributable to aluminum in the tetrahedral coordination state and typically associated with BASs, and a minor one at 0 ppm, attributable to extra-framework alumina (EFAL) in octahedral coordination. Peaks observed at 20 ppm are attributable to contamination from trace aluminum content of the NMR rotor, do not arise from the ZSM-5 sample, and are easily separated from the peaks of interest. Figure SI-4 in Supporting Information contains two-dimensional spectra used to guide quantitative NMR data interpretation. After treatment in hot liquid water, the intensity of the EFAL peak at 0 ppm increases and the intensity of the framework peak at 60 ppm decreases, a sign of Al conversion from tetrahedral BAS to octahedral EFAL. Qualitatively, the  $^{27}\text{Al}$  NMR spectra shown in Figure 4 are qualitatively similar to those obtained from analysis of ZSM-5 treated under steam or acid conditions.<sup>34, 36, 37</sup> Under steam and acid conditions, the conversion of tetrahedral to octahedral Al is attributed to

hydrolysis of Al-O, and the spectra in Figure 4 suggest the same process must occur under liquid water conditions.

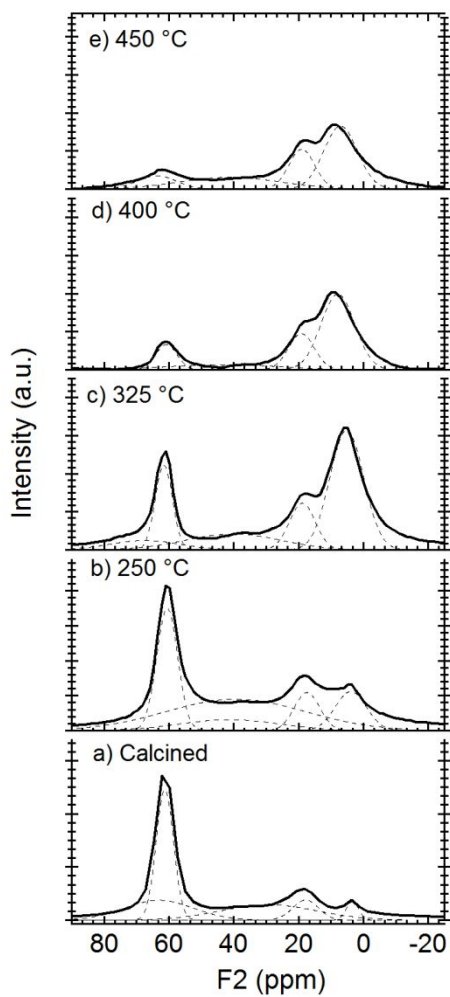


**Figure 4.** 1-D  $^{27}\text{Al}$  NMR spectra for a) untreated, b) 250 °C treated c) 325 °C treated, d) 400 °C treated, e) 450 °C treated ZSM-5 samples in hot liquid water.

Table 2 provides quantitative data obtained by integration of the  $^{27}\text{Al}$  NMR spectra shown in Figure 4. NMR analysis confirms that the Si/Al ratio is approximately 20:1 in the original sample. The bulk Si/Al ratio decreases with increasing treatment temperature, consistent with removal of internal Al during treatment resulting in an overall decrease in the bulk Al content of the sample. After treatment at 450 °C, Al content was less than the detection limit of the instrument (i.e., Si/Al > 700). In fact,  $^{29}\text{Si}$  NMR spectra of treated zeolite (See SI-4d in Supporting Information) resemble silicalite,<sup>38</sup> suggesting near quantitative dealumination of the MFI framework. Likewise, the ratio of tetrahedral (BAS) to octahedral (EFAL) sites decreases with increasing treatment temperature for temperatures less than 400 °C, from a ratio of 13.7 in the original sample to 0.16 in the sample treated at 400 °C, an 85-fold decrease. Interestingly, the ratio of tetrahedral to octahedral sites remain constant or even increase with increasing temperature from 400 to 450 °C, a finding that is similar to that observed for crystallinity and as shown in Figure 1b.

**Table 2.** Al coordination in liquid water treated ZSM-5 as estimated from  $^{27}\text{Al}$  NMR analysis.

Sample Temp ( $^{\circ}\text{C}$ )	$^{27}\text{Al}$ Tetrahedral Al sites	$^{27}\text{Al}$ Octahedral Al sites	$^{27}\text{Al}$ Si/Al ratio
Calcined	93.2	6.8	19.5
250	61.5	38.5	66.4
275	78.7	21.3	74.2
325	47.8	52.2	36.5
400	13.9	86.3	435.6
430	8	91	22
440	11	89	153.6
450	22.2	77.8	>700

NMR provides useful information on Al speciation in the bulk but provides no spatial information. XPS was used to quantify the change in near-surface aluminum content. Figure 5 presents XPS of the Al 2p region for calcined zeolite and for zeolite samples treated at 325 and 400  $^{\circ}\text{C}$ . Figure 5 demonstrates that the intensity of the Al 2p band (centered at 76.5 eV) increases monotonically with increasing treatment temperature from the “initial” value of the calcined sample. In contrast with the Al 2p features, spectra for the Si 2p photoelectron region that correspond to each respective scan in Figure 5 reveal only nominal changes as shown in Fig. SI-5 in the Supporting Information. Figure 5 provides quantified Si/Al ratios as determined from total feature areas for each Si 2p and

Al 2p spectral region after correction by instrument-specific sensitivity factors.<sup>39</sup> The estimated Si/Al ratio in the near surface region decreases from an initial value of 58 in the original sample to 4.3 after treatment at 400 °C. Considering the surface sensitivity of XPS, the decrease in the Si/Al ratio at the near surface is consistent with migration of aluminum atoms from the bulk to near-interfacial sites during liquid water treatment. Similar results have been reported previously after steam treatment of ZSM-5,<sup>34, 36, 40</sup> building on the similarities in NMR spectra mentioned previously.

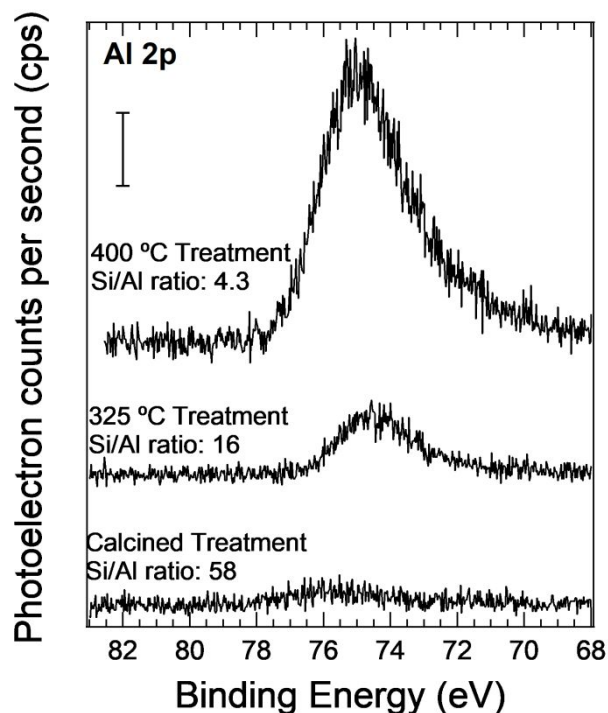


**Figure 5.** Al 2p XP spectra of untreated (bottom), 325 °C treated (middle), and 400 °C treated (top) ZSM-5 samples in hot liquid water. The corresponding surface Si/Al ratios

are inset into each respective spectrum. Scale bar represents 100 counts per second (cps) for all spectra.

The distribution of aluminum on the ZSM-5 surface was investigated using EDS. Images obtained using EDS, shown in Figure SI-5 of the Supporting Information, indicate increased Al density of ZSM-5 crystals treated at 250 and 325 °C, consistent with XPS analysis and similar to previous observations of steam-treated ZSM-5.<sup>34</sup> In contrast, the Al composition of the needles formed at 450 °C and observed using SEM is similar to that of the parent ZSM-5, suggesting that Al surface enrichment does not occur under the more aggressive temperature conditions. This observation may suggest that Al remains at the surface at milder conditions, but is solubilized into the continuous water phase at the more aggressive ones. Alternatively, it may suggest different temperature dependencies for the rates of de-crystallization and dealumination.

<sup>27</sup>Al NMR, XPS, and EDS are consistent with Al-O hydrolysis followed by Al migration to the zeolite surface. IR spectroscopy was used to examine the effects of liquid water treatment on proton coordination, including silanol (Si-OH) and the proton associated with

BASs. The IR spectrum of calcined ZSM-5, plotted in Figure 6, contains the expected bands characteristic of BASs ( $3618\text{ cm}^{-1}$ ) along with surface silanol groups ( $3746\text{ cm}^{-1}$ ).<sup>31, 41</sup> Interestingly, the BAS feature appears in the spectra obtained for samples treated at all temperatures, indicating the presence of acidic protons.<sup>34</sup> With increasing treatment temperature however, the intensity of the BAS band decreases in parallel with the appearance of a new band attributable to extra-framework alumina, EFAL, at  $3660\text{--}3690\text{ cm}^{-1}$ .<sup>42</sup> The decreasing intensity of the BAS band and the increasing intensity of the EFAL band is again consistent with the dealumination process suggested by NMR, XPS, and EDS. In contrast with the dramatic changes observed in the EFAL and Brønsted acid bands, the intensity of the silanol band remains relatively unchanged by treatment, consistent with previous studies of ZSM-5 behavior under dealuminating conditions that suggest that silanol defect formed after Al-O hydrolysis do not propagate through the structure.<sup>43, 44</sup>

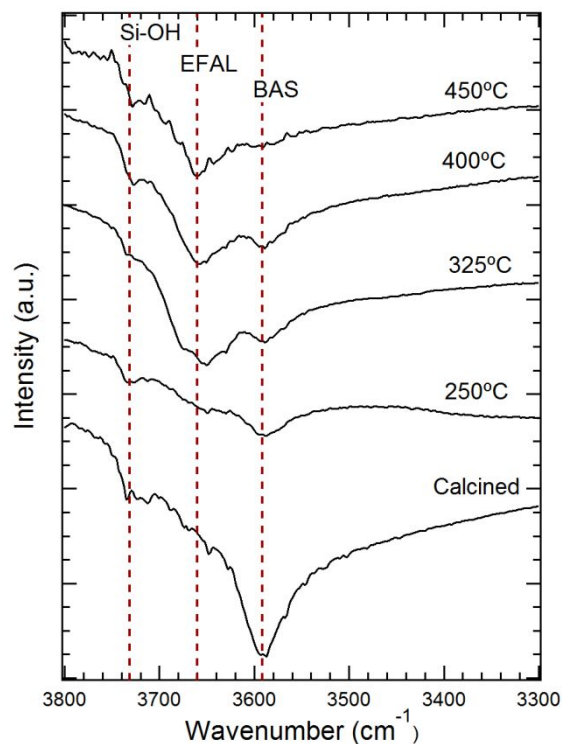


**Figure 6.** DRIFTS spectra of a) ZSM-5 untreated, b) 250 °C treated, c) 325 °C treated, d) 400 °C treated and e) 450 °C treated samples in hot liquid water

Lastly, pyridine-IR<sup>42</sup> and isopropylamine titration<sup>45</sup> were performed to quantify the ratio of BAS to Lewis acid sites (LAS) and the absolute densities of BASs and LASs in the treated samples. Figure SI-6 (in the Supporting Information) provides characteristic pyridine-IR spectra obtained from analysis of water-treated ZSM-5. Table 3 summarizes the results, showing that the ratio of BAS to LAS decreases from 9.8 for the calcined

material to 1.4 for ZSM-5 treated in liquid water at 450 °C. Isopropylamine titration<sup>45</sup> can be used to quantify BAS density in zeolites. Table 3 provides the results, showing that BAS density of the calcined sample is 570  $\mu\text{mol g}^{-1}$ , consistent with expectations.<sup>46-48</sup> After treatment in hot liquid water at 350 °C, the BAS density decreases by a factor of 3. Treatment at 450 °C reduces BAS density by nearly 98% compared to the calcined version. These results are consistent with those obtained from NMR and completely consistent with water-promoted dealumination.

**Table 3.** Acid properties of ZSM-5 after treatment in hot liquid water.

Sample Description	BAS <sup>a</sup> /LAS <sup>b,c</sup>	BAS density <sup>d</sup> ( $\mu\text{mol g}^{-1}$ )	LAS <sup>e</sup> density ( $\mu\text{mol g}^{-1}$ )
Calcined ZSM-5	9.8	570	58
ZSM-5 (350 °C)	3.8	167	44
ZSM-5 (450 °C)	1.4	14	10

<sup>a</sup> Brønsted acid site, BAS; <sup>b</sup> Lewis acid site, LAS; <sup>c</sup> BAS/LAS determined from pyridine FTIR; <sup>d</sup> BAS density determined directly from isopropylamine titration, <sup>e</sup> LAS density determined from pyridine FTIR and isopropylamine titration.

Conversion of tetrahedral Al to octahedral Al can result in formation of Lewis acid sites (LAS). Pyridine-IR and isopropyl amine titration were combined to quantify LAS densities. Table 3 provides quantitative results. Interestingly, trends observed in the  $^{27}\text{Al}$  NMR spectra contradict those observed for LAS density. Similar to the trends observed for BAS, the LAS density decreases with increasing liquid water treatment temperatures, as shown in Table 3. In contrast,  $^{27}\text{Al}$  NMR reveals a monotonic increase in octahedrally coordinated aluminum EFAL up to 400 °C. Kuel et al.<sup>33</sup> have shown a similar discrepancy between the acid site concentrations of steam treated BEA zeolite measured using  $^{27}\text{Al}$  NMR and ammonia TPD techniques. The discrepancy between  $^{27}\text{Al}$  NMR and ammonia TPD measurements is likely attributable to formation of inactive EFAL species, as noted previously by Loeffler et al.<sup>43</sup>

#### 4. Discussion

A major objective of this work was to evaluate the stability of ZSM-5 in hot liquid water over the temperature range explored in recent studies of catalytic upgrading of various biorenewable feeds.<sup>4-6, 8</sup> The experimental component of this study clearly indicates that ZSM-5 degradation follows a path consisting of both decrystallization and dealumination, and the available data provide some quantitative detail. XRD indicates that the framework retained >80% of its original crystallinity at all conditions, with unusual behavior observed at temperatures greater than the critical point of water. Similarly, N<sub>2</sub> sorption indicates retention of >60% of its original micropore area (as estimated using the  $t$ -plot method). These findings are both consistent with partial collapse of the MFI framework during treatment. Likewise, surface features including crystal thinning and the appearance of cavities observed using electron microscopy are similar to those reported after alkali promoted ZSM-5 desilication by Si-O bond hydrolysis.<sup>28, 29</sup> Unlike other zeolites, which undergo internal decrystallization and framework collapse when exposed to hot liquid water,<sup>11, 18</sup> only the external surfaces of MFI show signs of degradation, and the internal framework itself is relatively unperturbed during treatment. The surface degradation seen here is similar to alkali promoted desilication of ZSM-5, showing a second qualitative

similarity between hot liquid water and alkali treatments.<sup>28, 29, 49, 50</sup> Decrystallization therefore appears to be associated at least partially with desilication and by extension the hydrolysis of Si-O bonds.

In parallel with decrystallization, ZSM-5 undergoes a series of dealumination processes when contacted with hot liquid water. These processes presumably initiate with hydrolysis of tetrahedral Al-O bonds, followed by Al migration to the surface and subsequent deposition of octahedral aluminum as EFAL on the zeolite surface. Accordingly, liquid water treatment promotes ZSM-5 dealumination that follows a route similar to that reported previously for steaming conditions.<sup>34</sup> Whereas the MFI framework retains >80% of its original crystallinity after treatment in liquid water, BAS density decreases by >90%, suggesting that the dealumination rate is greater than the decrystallization rate.<sup>27</sup> The fact that silanol content remains constant despite varying levels of dealumination suggests that Al-O creates internal defects that do not propagate.<sup>34</sup> Presumably, silicon available from other sources reforms Si-O bonds that replace the Al-O bonds as they break, as has been suggested previously to explain the response of ZSM-5 to steam.<sup>34</sup>

Exposure of ZSM-5 to hot liquid water therefore leads to degradation phenomena that combine features previously observed separately under alkali<sup>30, 50-53</sup> and steaming conditions.<sup>33-35</sup> In fact, Groen et al.<sup>54</sup> showed that sequential alkali and steam treatments can be used to decouple desilication to form mesopores (alkali treatment) and dealumination for fine tuning of acid density and strength (steam treatment). Instead, hot liquid water promotes both desilication and dealumination in parallel with one another. In fact, the two processes may be coupled with one another to a certain extent, as formation of defects following dealumination may lead to subsequent desilication and crystallinity loss, though the integrity of internal lattice features indicates that this process does not result in complete collapse. The intimate details of these processes remain incompletely understood even under the relatively well studied conditions of alkali and steam treatment, and fully differentiating them in hot liquid water is beyond the scope of the present study. Nonetheless, the current study provides sufficient details for further analysis.

The available data provide guidance for interpretation of literature data on the use of ZSM-5 in hot liquid water and further can provide insight into zeolite-water interactions on

zeolite degradation. Addressing the issue of interpreting activity studies first, the  $^{27}\text{Al}$  NMR data indicate that conversion of catalytically active tetrahedral to EFAL octahedral sites occurs even under the mildest conditions considered here, treatment at 250 °C for 3 hours. Accordingly, most previous studies of ZSM-5 catalysis in hot liquid water were likely performed with material that had been partially dealuminated,<sup>3-6, 19</sup> likely explaining observations of reduced activity and reusability. That stated, the residual BASs likely remain accessible to reactants; in fact, the increased surface area and decreased crystal thickness may improve reactant access to BASs, similar to the findings of others after desilication.<sup>28, 52, 54</sup> Improved access may explain the observation of retained ZSM-5 activity under conditions that should have resulted in greater than 90% dealumination. Many previous studies have investigated the use of ZSM-5 for conversion of bulky reactants such as cis-alkenes or highly branched fatty acids<sup>5</sup> or poorly defined mixtures potentially consisting of similar compounds.<sup>4, 6</sup> For sterically hindered compounds, reaction inside ZSM-5 is likely to be diffusion limited, meaning that improved access can reasonably be expected to partially offset BAS loss.

Unfortunately, the long-term outcome of the dealumination process under industrial conditions will be complete depletion of BAS, resulting in irreversible catalyst deactivation. That stated, various approaches including surface hydrophobization (HY)<sup>13</sup> and internal defect healing ( $\beta$ )<sup>18</sup> have been shown to extend the stability of other zeolites in hot liquid water. Similar approaches have not been examined for ZSM-5, but might be investigated in future work. To guide efforts to improve ZSM-5 stability in hot liquid water, the current data were re-analyzed to understand the role of water-zeolite interactions on zeolite degradation.

While the aforementioned conclusions regarding decrystallization and dealumination seem clear, the available data show an additional interesting feature that requires explanation. As expected, decrystallization and dealumination are both functions of temperature. However, the extent of decrystallization and dealumination does not increase with increasing temperature over the entire range considered. In both cases, unusual behavior was observed in the vicinity of the critical point. Modeling zeolite degradation as a chemically activated process would suggest degradation rates should follow Arrhenius behavior, i.e., zeolite degradation (both decrystallization and

dealumination) should increase monotonically with increasing temperature, instead of the observed behavior near the critical point. Although previous studies of zeolite stability did not probe the near-critical temperature range, several studies on molecular chemistry in supercritical water provide insight. Specifically, hydrolysis of C-O<sup>55, 56</sup> and C-Cl<sup>57, 58</sup> bonds exhibits rate behavior near the critical point that is qualitatively similar to the degradation phenomena observed here, i.e., increasing the temperature does not result in the expected increase in reaction rates. For molecular reactions, water auto-ionization<sup>55, 56</sup> to form H<sub>3</sub>O<sup>+</sup> and OH<sup>-</sup> as well as transition state solvation<sup>57, 58</sup> were used to explain the near-critical phenomena. Since both desilication (Si-O and possibly Al-O) and dealumination (Al-O) involve bond hydrolysis, similar phenomena might plausibly explain the non-Arrhenius behavior observed here for ZSM-5 degradation, motivating further consideration.

The key to understanding zeolite-water interactions is the temperature dependence of water's thermodynamic properties.  $K_w$  – the equilibrium constant governing auto-ionization of water to produce H<sup>+</sup> and OH<sup>-</sup> and the dielectric constant  $\epsilon$  – a typical parameter used to describe the polarity of a solvent – both vary dramatically and non-

linearly with increasing temperature. Specifically,  $K_w$  increases over the temperature range from 25 to 300 °C from its familiar value of  $1 \times 10^{-14}$  to a maximum of approximately  $1 \times 10^{-10}$ . Correspondingly, the pH of neutral water at 300 °C is approximately 5, meaning that concentrations of both  $H^+$  and  $OH^-$  are 100× greater than at room temperature. For temperatures greater than 300 °C,  $K_w$  monotonically decreases with increasing temperature, taking a value of  $1 \times 10^{-17}$  at 450 °C.<sup>24</sup> Similarly, the value of  $\epsilon$  smoothly decreases from its familiar value of 78 at 25 °C to 1 at 450 °C, meaning that supercritical water is a poor solvent for salts but an excellent solvent for nonpolar compounds.<sup>1</sup> The temperature dependence of these important thermodynamic properties affects many phenomena and specifically has been suggested as the root cause for the non-Arrhenius rate phenomena observed previously for C-O and C-Cl hydrolysis.<sup>55-58</sup>

Hydrolysis of Si-O and Al-O bonds is analogous to C-O and C-Cl hydrolysis, meaning that the temperature dependence of  $K_w$  and  $\epsilon$  might plausibly be expected to impact zeolite decrystallization and dealumination rates. Water auto-ionization is almost certainly important as studies on alkali promoted desilication<sup>51, 52</sup> and acid-promoted dealumination<sup>37</sup> establish the role of pH on zeolite degradation. Transition state solvation

might also be important in Si-O and Al-O bond hydrolysis, as suggested by theoretical work on Si-O bond cleavage in silanols.<sup>59</sup> Previous studies on zeolite degradation have not considered acid/base effects and transition state solvation, probably because they have not examined the large temperature range studied here. However, over the large temperature range of study permitted by ZSM-5, the temperature dependence of water's thermodynamic properties must be considered. Rigorous analysis requires rate constants, and extracting rate constants from the available data was therefore the next step in this study.

Data were obtained in this study at a single time over a range of temperatures, making determination of rate constants non-obvious. Fortunately, prior work that included transient measurements suggests that zeolite degradation may often follow a pseudo-first order rate law. In fact, re-plotting data reported by Ravenelle et al.<sup>11</sup> as shown in Figure SI-7 indicates that the assumption of first-order degradation kinetics is a reasonable one. Theoretical considerations by Hartman and Fogler<sup>60, 61</sup> lead to a similar conclusion. Modeling the degradation rate law as first order allows the single measured time point to be used to estimate apparent degradation rate constants ( $k_{app}$ ) over the entire

temperature range of this study. Based on all prior consideration, analyses were performed for decrystallization rates, using crystallinity data shown in Figure 1b and with the understanding that both desilication and dealumination may play a role in decrystallization behavior. Dealumination rates were estimated using the  $^{27}\text{Al}$  NMR data shown in Table 2. The corresponding values of  $k_{app}$  estimated for decrystallization and dealumination are provided in Table SI-1.

Having extracted values of decrystallization and dealumination rate constants, a simple Arrhenius analysis was performed using the familiar expression:

$$\ln(k_{app}) = \ln(A) - \frac{E_a}{RT} \quad (1)$$

where  $E_a$  is the activation energy of degradation,  $A$  is a pre-exponential factor,  $R$  is the gas constant, and  $T$  is temperature. Figure 7a plots ZSM-5 decrystallization rate constants (black squares), revealing the non-Arrhenius temperature relationship anticipated by the qualitative features presented in Figure 1b. Statistically, the simple Arrhenius model is a poor fit to the available data ( $r^2 = 0.75$ ), and more specifically the Arrhenius models shows systematic error in the vicinity of the critical point. In addition,

the estimated activation energy of  $45 \pm 23 \text{ kJ mol}^{-1}$  is much less than expected,<sup>62</sup> even after accounting for the considerable experimental uncertainty. Similarly, the Arrhenius analysis of the dealumination rate constant, plotted in Figure 7a as red circles, shows noticeable deviation from linearity at  $T \geq 400 \text{ }^\circ\text{C}$  and the corresponding estimate of dealumination activation energy is much less than expected.<sup>62</sup>

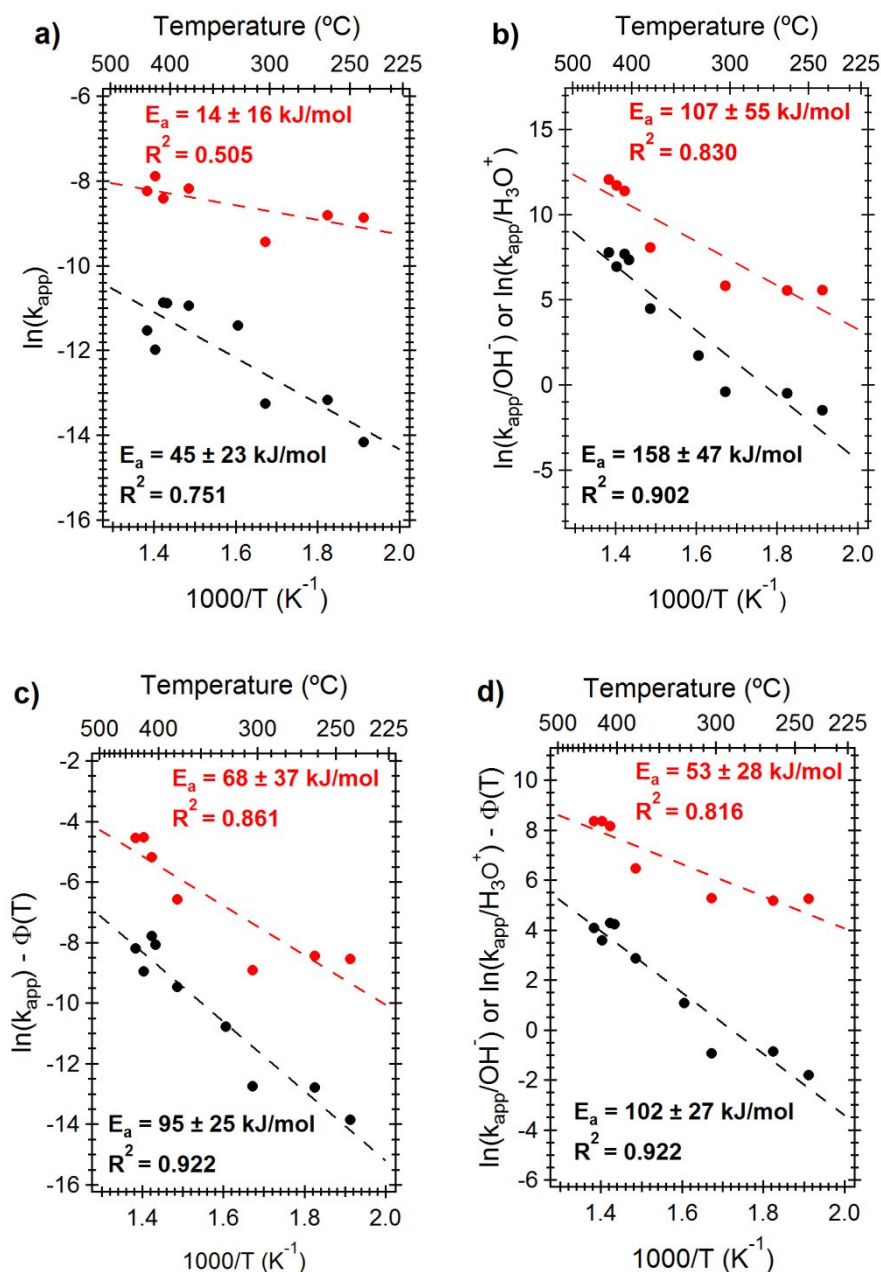


**Figure 7.** Plots of ZSM-5 degradation rates of both decrystallization (black circles) and dealumination (red circles) a) using a simple Arrhenius analysis, b) an adjusted Arrhenius analysis assuming water as the sole source of OH<sup>-</sup> or H<sup>+</sup> and accounting for the temperature dependence of  $K_w$ , c) an adjusted Arrhenius analysis accounting for the

temperature dependence of dielectric constant using the Kirkwood correlation factor, and  
 d) an adjusted Arrhenius analysis accounting for the temperature dependence of both  $K_W$   
 and dielectric constant.

The non-Arrhenius temperature dependence on zeolite degradation shown in Figure 7a suggests that the effect of temperature is more subtle than the usual thermal effect. Literature models describing the role of water on the rates of molecular reactions were used to guide modification of the Arrhenius expression to account for the temperature dependence of water's thermodynamic properties, specifically  $K_W$  and  $\epsilon$ . To account for the role of water auto-ionization on the rate of acid-catalyzed C-O hydrolysis, Taylor et al.<sup>56</sup> proposed the following modification to the Arrhenius expression:

$$-\frac{d[X(t)]}{dt} = k_{app}[X(t)] = A \cdot \exp\left[\frac{E_a}{RT}\right] \{[H^+] \text{ or } [OH^-]\} [X(t)] \quad (2, \text{ based on Ref. } 55)$$

where  $X(t)$  is the reactant concentration and  $[H^+] = [OH^-] \approx K_W^{1/2}$ . In the derivation of Equation (2), Taylor et al.<sup>55</sup> assumed that the activity coefficients of  $H^+$  and  $OH^-$  are approximately 1. Rearrangement of Equation (2) yields:

$$\ln\left(\frac{k_{app}}{[H^+] \text{ or } [OH^-]}\right) = \ln(A) + \frac{E_a}{RT} \quad (3)$$

Equation (3) suggests plotting  $k_{\text{app}}$  data after normalization by  $[\text{H}^+]$ ,  $[\text{OH}^-]$ , or possibly the sum of the two – depending on whether the pathway is acid or base catalyzed. In fact, desilication is generally base catalyzed<sup>52</sup> and dealumination can be acid catalyzed, meaning that both  $[\text{H}^+]$  and  $[\text{OH}^-]$  can plausibly influence degradation rates. Fortunately, in neutral water  $[\text{H}^+] = [\text{OH}^-]$ , making the distinction unnecessary here. Figure 7b presents the results of this analysis for decrystallization (black squares) and for dealumination (red circles). In contrast with the Arrhenius analysis, the trend line obtained for decrystallization using the modified Arrhenius expression is linear over the entire data set ( $r^2 = 0.90$ ), and data at temperatures greater and less than the critical point are equally well fit. The slope of the best-fit decrystallization trend line corresponds to an activation energy of  $160 \pm 50 \text{ kJ mol}^{-1}$ , which is in reasonable agreement calculated values of the activation energy of Si–O bond hydrolysis.<sup>62</sup> As with decrystallization, the modified Arrhenius analysis of the dealumination data (red circles) results in a linear trend, with improved fitting statistics. Quantitatively, the modified analysis yields a dealumination activation energy of  $110 \pm 60 \text{ kJ mol}^{-1}$ , which is in reasonable agreement but somewhat less than the value of 190–260  $\text{kJ mol}^{-1}$  estimated using DFT.<sup>62</sup> In fact, the DFT calculation

was performed in vacuum and did not account for solvation effects or defects, meaning that the DFT estimate is expected to be greater than can be observed experimentally – as found here.

Although incorporating  $K_W$  effects in the rate analysis greatly improves the quality of the fit, the resulting fits are not perfect and exhibit evidence of systematic discrepancies that indicate that including  $[H^+]$  and  $[OH^-]$  in the analysis may not be sufficient. Realizing that Si-O and Al-O hydrolysis must play important roles in decrystallization and dealumination further suggests examining the transition state solvation effect of water. In cases where the transition state is more polar than the reactants, a polar solvent can stabilize the transition state and increase reaction rates.<sup>63, 64</sup> Marrone et al.<sup>58</sup> invoked this phenomenon and the temperature varying value of  $\varepsilon$  to explain their measurements of C-Cl hydrolysis rates in near and supercritical water.

To test the effect of transition state solvation on degradation rates, a new form of the Arrhenius expression was adopted following the analysis by Marrone et al.<sup>58</sup>

$$\ln(k_{app}) = \ln(A) - \frac{E_A}{RT} + \left[ \frac{1-\varepsilon}{2+\varepsilon} \right] \frac{\varphi}{T} \quad (4)$$

where  $\varphi$  is related to the differences in the dipole moments of the reactants and transition state. For molecular reactions,  $\varphi$  is well defined. Unfortunately, for zeolite degradation,  $\varphi$  is not known. Instead,  $\varphi$  was used as an additional fitting parameter to determine if the form of Equation (4) could afford a better fit of the available data than either Equation (1) or (3). Figure 7c contains plots of the decrystallization (black squares) and dealumination (red circles) rate constants analyzed using the Arrhenius expression shown in Equation (4). Statistically, Equation (4) provides similar fits to the available data as does Equation (3), despite the use of an additional fitting parameter. However, the corresponding activation energies for decrystallization ( $95 \pm 25 \text{ kJ mol}^{-1}$ ) and dealumination ( $68 \pm 37 \text{ kJ mol}^{-1}$ ) determined using Equation (4) are in poor agreement with expected values.<sup>65</sup> Accordingly, the results of the analysis shown in Figure 7c suggest that including transition state solvation on its own cannot explain the non-Arrhenius rate behavior observed here.

The final logical analysis is to combine the  $[\text{OH}^-]$  or  $[\text{H}^+]$  correction with the transition state solvation approach, resulting in a third modified form of the Arrhenius expression:

$$\ln\left(\frac{k_{app}}{[H^+] \text{ or } [OH^-]}\right) = \ln(A) - \frac{E_A}{RT} + \left[\frac{1-\varepsilon}{2+\varepsilon}\right]\frac{\varphi}{T} \quad (5)$$

where all variables have been previously defined. Figure 7d contains Arrhenius-style plots of decrystallization (black squares) and dealumination (red circles) rate constants, analyzed as suggested in Equation (4). In both cases, including  $K_W$  and  $\varepsilon$  correction terms results in modest improvement in fitting coefficients, but again with the undesired effect of decreasing the apparent activation energies. Accordingly, the available data cannot justify the model indicated by Equation (5).

Based on the analysis shown in Figure 7, the temperature dependence of  $K_W$  must be included in analysis of decrystallization and dealumination rates. Adding the  $\varepsilon$  correction term does not yield sufficient benefits to justify including it in the analysis. This may indicate that the effective dielectric constant of water that solvates the Si-O and/or Al-O transition states is not the same as in the bulk, an observation which could be suggestive of confinement<sup>66</sup> or surface-mediation effects on  $\varepsilon$ .<sup>67</sup> Future work is recommended to examine the thermodynamic state of water in zeolite micropores, especially since it may play important roles in reactant diffusion and catalyst activity.<sup>68</sup>

The present analysis can guide future approaches to prolong zeolite lifetimes in hot liquid water. As a general statement, acid site loss by dealumination is a more pressing concern than decrystallization, since conditions under which >80% of the initial crystallinity is retained correspond to >90% decrease in BAS. Furthermore, the temperature range from 300 to approximately 400 °C should be avoided as the most aggressive degradation behavior is observed here. Most prior tests of ZSM-5 catalysis involve batch reactors. Unless special precautions are taken, operation under batch conditions means that even when the final temperature is  $\geq 400$  °C, the zeolite will encounter aggressively degrading conditions during heat up (and cool down). In fact, the experiments shown here were carefully performed under flow conditions to avoid this problem. Accordingly, future activity tests at temperature  $\geq 400$  °C should consider use of conditions that minimize zeolite contact with liquid water before reaching reaction temperature.

Aside from avoiding a certain temperature range, the composition of the reaction mixture might be modified to improve ZSM-5 stability. For example, addition of dilute hydrochloric acid could be used to decrease decrystallization rates, consistent with the

study by Ennaert et al.<sup>12</sup> On the other hand, addition of acid to limit decrystallization runs the risk of increasing dealumination rates, since dealumination can be acid promoted. Alternatively, since  $K_w$  and possibly  $\varepsilon$  influence degradation rates, nonpolar cosolvents can be used to extend catalyst lifetime. Although mixture data are not available at elevated temperatures, the effect of adding nonpolar cosolvent can reasonably be expected to decrease both  $K_w$  and  $\varepsilon$ , effectively making water less aggressive. Likewise, addition of cosolvents might be effective in reducing the chemical potential of water, which might have similar benefits. Indeed, several previous groups may have inadvertently used the cosolvent approach by studying zeolite activity under conditions where a significant hydrocarbon cosolvent was present as a reactant.<sup>7, 69, 70</sup> Future work should study the cosolvent approach under rigorously defined conditions.

## 5. Conclusion

Many previous studies investigate ZSM-5 catalysis in the presence of liquid phase water at temperatures where catalyst stability were not then available. To address this knowledge gap, ZSM-5 degradation was studied in liquid water at temperatures over the

range from 250 to 450 °C, with specific emphasis on the effect of zeolite-water interactions on crystallinity, textural properties, Al content and coordination, and BAS and LAS densities. The crystallinity of the ZSM-5 framework remains constant for up to 3 hours when treated in hot liquid water at temperatures <325 °C. When treated at temperatures greater than 325 °C, ZSM-5 crystallinity decreases and textural properties show signs of framework degradation. The temperature dependence of crystallinity and changes in textural properties are non-monotonic, with the range from 300-400 °C being the most aggressive conditions studied. Comparison of SEM and STEM images suggest that ZSM-5 decrystallization initiates primarily at the crystal surface. Characterization using a variety of techniques indicate that treatment in hot liquid water promotes Al-O bond hydrolysis, followed by Al migration to the surface, and finally deposition as EFAL. Under some conditions, even the surface Al may be removed by the hot liquid water treatment. Again, Al characterization suggested that temperatures in the range from 300-400 °C were the most aggressive. These findings likely explain reports of activity loss and poor reusability when ZSM-5 is used as a catalyst in hot liquid water.

The experimental data suggest that ZSM-5 degradation proceeds via parallel desilication and dealumination pathways, combining aspects previously associated separately to alkali and steam treatments. Crystallinity (XRD) and dealumination ( $^{27}\text{Al}$  NMR) data were analyzed using a first-order kinetic model to estimate apparent degradation rate constants as functions of temperature. The temperature dependencies of the decrystallization and dealumination rate constants were analyzed and found not to follow typical Arrhenius behavior, suggesting that temperature plays more than a thermal role in determining ZSM-5 degradation rates. Several different modifications of the Arrhenius equation were evaluated to capture the effects of water solvation and auto-ionization to produce  $\text{H}^+$  and  $\text{OH}^-$  on degradation rate. Of these models, including the effect of water auto-ionization appeared the most promising in terms of statistical fit to the available data and agreement of activation energies with expected values. This analysis thereby explains the non-Arrhenius relationship found for ZSM-5 degradation and suggests that future work on ZSM-5 catalysis in liquid water avoid the temperature range from 300-400 °C or add nonpolar solvents to the reaction mixture if possible.

## Associated Content

## Supporting Information

The Supporting Information file is available free of charge on the Royal Society of Chemistry website.

## Corresponding Author

\*Email: mttimko@wpi.edu. Phone: +1-508-831-4101.

## Acknowledgements

We thank Saudi Aramco (6600023444) and the ACS Petroleum Research Fund (54912-DNI9) for supporting this work. The U.S. National Science Foundation supported MTT's contribution to this work (award #1554238). JQB and XH thank the U.S. National Science Foundation for their contributions (award # 1605114). ARM thanks the Carl and Inez Weidenmiller Fellowship for fellowship support for a portion of this work. WPI provided start-up funds to establish the catalyst stability test facility. Doug White and Richard Sisson supported SEM activities. Jeffrey Rimer and Thuy Thanh Le (both at University of Houston) provided helpful comments during the manuscript revision process.

## 5. References

1. A. A. Peterson, F. Vogel, R. P. Lachance, M. Fröling, J. Antal, Michael J. and J. W. Tester, *Energy & Environmental Science*, 2008, **1**, 32.
2. S. S. Toor, L. Rosendahl, A. Rudolf, S. Sohail, L. Rosendahl, A. Rudolf, S. S. Toor, L. Rosendahl and A. Rudolf, *Energy*, 2011, **36**, 2328-2342.
3. T. Robin, J. M. Jones and A. B. Ross, *Biomass and Bioenergy*, 2017, **98**, 26-36.
4. P. Duan, Y. Xu, F. Wang, B. Wang and W. Yan, *Biochemical Engineering Journal*, 2016, **116**, 105-112.
5. N. Mo and P. E. Savage, *ACS Sustainable Chemistry and Engineering*, 2014, **2**, 88-94.
6. Z. Li and P. E. Savage, *Algal Research*, 2013, **2**, 154-163.
7. A. K. Deepa and P. L. Dhepe, *ACS Catalysis*, 2015, **5**, 365-379.
8. N. Mo, W. Tandar and P. E. Savage, *Journal of Supercritical Fluids*, 2015, **102**, 73-79.
9. H. Xiong, H. N. Pham and A. K. Datye, *Green Chemistry*, 2014, **16**, 4627-4643.
10. W. Lutz, H. Toufar, R. Kurzhals and M. Suckow, *Adsorption*, 2005, **11**, 405-413.
11. R. M. Ravenelle, F. Schübler, A. Damico, N. Danilina, J. A. Van Bokhoven, J. A. Lercher, C. W. Jones and C. Sievers, *Journal of Physical Chemistry C*, 2010, **114**, 19582-19595.
12. T. Ennaert, J. Geboers, E. Gobechiya, C. M. Courtin, M. Kurttepel, K. Houthoofd, C. E. A. Kirschhock, P. C. M. M. Magusin, S. Bals, P. A. Jacobs and B. F. Sels, *ACS Catalysis*, 2015, **5**, 754-768.
13. P. A. Zapata, Y. Huang, M. A. Gonzalez-Borja and D. E. Resasco, *Journal of Catalysis*, 2013, **308**, 82-97.
14. W. Lutz, W. Gessner, R. Bertram, I. Pitsch and R. Fricke, *Microporous Materials*, 1997, **12**, 131-139.
15. I. A. Bakare, O. Muraza, T. Kurniawan, Z. H. Yamani, E. N. Shafei, A. K. Punetha, K. H. Choi and T. Yokoi, *Microporous and Mesoporous Materials*, 2016, **233**, 93-101.
16. A. K. Jamil, O. Muraza, R. Osuga, E. N. Shafei, K. H. Choi, Z. H. Yamani, A. Somali and T. Yokoi, *Journal of Physical Chemistry C*, 2016, **120**, 22918-22926.

17. L. Zhang, K. Chen, B. Chen, J. L. White and D. E. Resasco, *Journal of the American Chemical Society*, 2015, **137**, 11810-11819.
18. A. Vjunov, J. L. Fulton, D. M. Camaioni, J. Z. Hu, S. D. Burton, I. Arslan and J. A. Lercher, *Chemistry of Materials*, 2015, **27**, 3533-3545.
19. A. Zaker, P. Guerra, Y. Wang, G. Tompsett, X. Huang, J. Bond and M. T. Timko, *Catalysis Today*, 2018.
20. D. W. Gardner, J. Huo, T. C. Hoff, R. L. Johnson, B. H. Shanks and J.-p. P. Tessonier, *ACS Catalysis*, 2015, **5**, 4418-4422.
21. J. S. Kruger, V. Nikolakis and D. G. Vlachos, *Applied Catalysis A: General*, 2014, **469**, 116-123.
22. D. P. Serrano, R. A. García, M. Linares and B. Gil, *Catalysis Today*, 2012, **179**, 91-101.
23. K. Muraoka, W. Chaikittisilp and T. Okubo, *Journal of the American Chemical Society*, 2016, **138**, 6184-6193.
24. A. V. Bandura and S. N. Lvov, *Journal of Physical and Chemical Reference Data*, 2006, **35**, 15-30.
25. ASTM, *ASTM International: D4758-01*, 2015, **05**, 3-5.
26. R. A. Beyerlein, C. Choi-Feng, J. B. Hall, B. J. Huggins and G. J. Ray, *Topics in Catalysis*, 1997, 27-42.
27. D. Fodor, A. Beloqui Redondo, F. Krumeich and J. A. Van Bokhoven, *Journal of Physical Chemistry C*, 2015, **119**, 5447-5453.
28. J. C. Groen, L. A. A. Peffer, J. A. Moulijn and J. Pérez-Ramírez, *Chemistry - A European Journal*, 2005, **11**, 4983-4994.
29. T. Sano, Y. Nakajima, Z. B. Wang, Y. Kawakami, K. Soga and A. Iwasaki, *Microporous Materials*, 1997, **12**, 71-77.
30. D. Fodor, F. Krumeich, R. Hauert and J. A. Van Bokhoven, *Chemistry - A European Journal*, 2015, **21**, 6272-6277.
31. C. S. Triantafillidis, A. G. Vlessidis, L. Nalbandian and N. P. Evmiridis, *Microporous and Mesoporous Materials*, 2001, **47**, 369-388.
32. B. C. LIPPENS and J. H. Boer, *Journal of Catalysis*, 1965, **4**, 319-323.

33. G. H. Kuehl and H. K. C. Timken, *Microporous and Mesoporous Materials*, 2000, **35**, 521-532.
34. J. Datka, S. Marschmeyer, T. Neubauer, J. Meusinger, H. Papp, F.-W. Schütze and I. Szpyt, *The Journal of Physical Chemistry*, 1996, **100**, 14451-14456.
35. M. Niwa, S. Sota and N. Katada, *Catalysis Today*, 2012, **185**, 17-24.
36. S. M. Campbell, D. M. Bibby, J. M. Coddington and R. F. Howe, *Journal of Catalysis*, 1996, **358**, 350-358.
37. P. J. J. Kooyman, P. van der Waal and H. Van Bekkum, *Zeolites*, 1997, **18**, 50-53.
38. C. a. Fyfe, G. C. Gobbi and G. J. Kennedy, *Journal of Physical Chemistry*, 1984, **88**, 3248-3253.
39. D. Briggs, *Surface and Interface Analysis*, 1981.
40. S. Marschmeyer and H. Papp, *Surface and Interface Analysis*, 1997, **25**, 660-666.
41. M. Trombetta, T. Armaroli, a. G. Alejandre, J. R. Solis and G. Busca, *Applied Catalysis A: General*, 2000, **192**, 125-136.
42. F. Jin and Y. Li, *Catalysis Today*, 2009, **145**, 101-107.
43. E. Loeffler, U. Lohse, C. Peuker, G. Oehlmann, L. M. Kustov, V. L. Zholobenko and V. B. Kazansky, *Zeolites*, 1990, **10**, 266-271.
44. S. Kumar, A. K. Sinha, S. G. Hegde and S. Sivasanker, *Journal of Molecular Catalysis A: Chemical*, 2000, **154**, 115-120.
45. W. E. Farneth and R. J. Gorte, *Chemical Reviews*, 1995, **95**, 615-635.
46. A. B. Kellicutt, R. Salary, O. A. Abdelrahman and J. Q. Bond, *Catalysis Science & Technology*, 2014, **4**, 2267.
47. F. Ferreira Madeira, K. Ben Tayeb, L. Pinard, H. Vezin, S. Maury and N. Cadran, *Applied Catalysis A: General*, 2012, **443-444**, 171-180.
48. K. Mlekodaj, K. Sadowska, J. Datka, K. G??ra-Marek and W. a. Makowski, *Microporous and Mesoporous Materials*, 2014, **183**, 54-61.
49. J. A. Van Bokhoven, D. C. Koningsberger, P. Kunkeler, H. Van Bekkum and A. P. M. Kentgens, *Journal of the American Chemical Society*, 2000, **122**, 12842-12847.
50. L. Su, L. Liu, J. Zhuang, H. Wang, Y. Li, W. Shen, Y. Xu and X. Bao, *Catalysis Letters*, 2003, **91**, 155-168.

51. M. Ogura, S. Y. Shinomiya, J. Tateno, Y. Nara, M. Nomura, E. Kikuchi and M. Matsukata, *Applied Catalysis A: General*, 2001, **219**, 33-43.
52. J. C. Groen, S. Abelló, L. A. Villaescusa and J. Pérez-Ramírez, *Microporous and Mesoporous Materials*, 2008, **114**, 93-102.
53. D. Verboekend and J. Pérez-Ramírez, *Catalysis Science & Technology*, 2011, **1**, 879.
54. J. C. Groen, J. A. Moulijn and J. Pérez-Ramírez, *Microporous and Mesoporous Materials*, 2005, **87**, 153-161.
55. J. D. Taylor, J. I. Steinfeld and J. W. Tester, *Industrial & Engineering Chemistry Research*, 2001, **40**, 67-74.
56. J. Taylor, F. Pacheco, J. Steinfeld and J. Tester, *Industrial & Engineering Chemistry Research*, 2002, **41**, 1-8.
57. D. Salvatierra, J. D. Taylor, P. A. Marrone and J. W. Tester, *Industrial & engineering chemistry research*, 1999, **38**, 4169-4174.
58. P. Marrone, T. Arias, W. Peters and J. Tester, *The Journal of Physical Chemistry A*, 1998, **102**, 7013-7028.
59. M. Cypryk and Y. Apeloig, *Organometallics*, 2002, **21**, 2165-2175.
60. R. L. Hartman and H. S. Fogler, *Industrial & engineering chemistry research*, 2005, **44**, 7738-7745.
61. R. L. Hartman and H. S. Fogler, *Langmuir*, 2007, **23**, 5477-5484.
62. S. Malola, S. Svelle, F. L. Bleken and O. Swang, *Angewandte Chemie - International Edition*, 2012, **51**, 652-655.
63. S. H. Townsend, M. A. Abraham, G. L. Huppert, M. T. Klein and S. C. Paspek, *Industrial and Engineering Chemistry Research*, 1988, **27**, 143-149.
64. M. W. Wong, M. J. Frisch and K. B. Wiberg, *J. Am. Chem. Soc.*, 1991, **113**, 4776-4782.
65. M. C. Silaghi, C. Chizallet and P. Raybaud, *Microporous and Mesoporous Materials*, 2014, **191**, 82-96.
66. K. V. Agrawal, S. Shimizu, L. W. Drahushuk, D. Kilcoyne and M. S. Strano, *Nature nanotechnology*, 2017, **12**, 267.
67. G. Makov and A. Nitzan, *The Journal of Physical Chemistry*, 1994, **98**, 3459-3466.

68. N. S. Gould and B. Xu, *Chemical science*, 2018, **9**, 281-287.
69. R. Sahu and P. L. Dhepe, *ChemSusChem*, 2012, **5**, 751-761.
70. R. O'Neil, M. N. Ahmad, L. Vanoye and F. Aiouache, *Industrial and Engineering Chemistry Research*, 2009, **48**, 4300-4306.